

# Mode switching in a multi-wavelength distributed feedback quantum cascade laser using an external micro-cavity

Cite as: Appl. Phys. Lett. **104**, 051102 (2014); <https://doi.org/10.1063/1.4863663>

Submitted: 24 November 2013 . Accepted: 13 January 2014 . Published Online: 03 February 2014

Meinrad Sidler, Patrick Rauter, Romain Blanchard, Pauline Métivier, Tobias S. Mansuripur, Christine Wang, Yong Huang, Jae-Hyun Ryou, Russell D. Dupuis, Jérôme Faist, and Federico Capasso



View Online



Export Citation



CrossMark

## ARTICLES YOU MAY BE INTERESTED IN

[Electrically tunable terahertz quantum cascade lasers based on a two-sections interdigitated distributed feedback cavity](#)

Applied Physics Letters **106**, 131107 (2015); <https://doi.org/10.1063/1.4916653>

[Surface emitting multi-wavelength array of single frequency quantum cascade lasers](#)

Applied Physics Letters **106**, 071104 (2015); <https://doi.org/10.1063/1.4913203>

[Single-mode tapered quantum cascade lasers](#)

Applied Physics Letters **102**, 181102 (2013); <https://doi.org/10.1063/1.4804261>

Lock-in Amplifiers  
up to 600 MHz



## Mode switching in a multi-wavelength distributed feedback quantum cascade laser using an external micro-cavity

Meinrad Sidler,<sup>1,2</sup> Patrick Rauter,<sup>1</sup> Romain Blanchard,<sup>1</sup> Pauline Métivier,<sup>1</sup> Tobias S. Mansuripur,<sup>3</sup> Christine Wang,<sup>4</sup> Yong Huang,<sup>5</sup> Jae-Hyun Ryou,<sup>5</sup> Russell D. Dupuis,<sup>5</sup> Jérôme Faist,<sup>2</sup> and Federico Capasso<sup>1,a)</sup>

<sup>1</sup>*School of Engineering and Applied Sciences, Harvard University, 29 Oxford St., Cambridge, Massachusetts 02138, USA*

<sup>2</sup>*Institute for Quantum Electronics, ETH Zurich, Wolfgang-Pauli-Strasse 16, 8093 Zurich, Switzerland*

<sup>3</sup>*Department of Physics, Harvard University, 17 Oxford St., Cambridge, Massachusetts 02138, USA*

<sup>4</sup>*MIT Lincoln Laboratory, 244 Wood St., Lexington, Massachusetts 02420, USA*

<sup>5</sup>*Center for Compound Semiconductors and School of Electrical and Computer Engineering, Georgia Institute of Technology, Atlanta, Georgia 30332-0250, USA*

(Received 24 November 2013; accepted 13 January 2014; published online 3 February 2014)

We demonstrate a multi-wavelength distributed feedback (DFB) quantum cascade laser (QCL) operating in a lensless external micro-cavity and achieve switchable single-mode emission at three distinct wavelengths selected by the DFB grating, each with a side-mode suppression ratio larger than 30 dB. Discrete wavelength tuning is achieved by modulating the feedback experienced by each mode of the multi-wavelength DFB QCL, resulting from a variation of the external cavity length. This method also provides a post-fabrication control of the lasing modes to correct for fabrication inhomogeneities, in particular, related to the cleaved facets position. © 2014 AIP Publishing LLC. [<http://dx.doi.org/10.1063/1.4863663>]

Quantum cascade lasers (QCLs) are compact, flexible, and powerful mid-infrared radiation source, for applications ranging from infrared spectroscopy<sup>1</sup> to free-space communication<sup>2</sup> and military countermeasures. Their active regions can be designed to have gain over a broad bandwidth<sup>3,4</sup> and wavelength tuning across the latter can be achieved using an external cavity (EC) with a diffraction grating providing wavelength specific feedback.<sup>5</sup> Alternative to EC-QCLs, a powerful and compact monolithic solution is offered by the use of an array of distributed feedback (DFB) QCLs.<sup>6</sup> Very high peak output power has recently been achieved by an array of DFB QCLs integrated with optical amplifiers.<sup>7</sup> However, emitter arrays require high fabrication yield and beam combining optics. Multi-section sampled grating QCLs,<sup>8</sup> coupled DFB QCLs,<sup>9</sup> and coupled Fabry-Perot cavities<sup>10</sup> have also been investigated for both discrete and continuous wavelength tuning.

For some spectroscopic applications, covering a discrete number of narrow spectral ranges is sufficient to unambiguously identify the chemical compound of interest, and continuous tuning of the source over a broad spectrum is not always required. Recently, simultaneous emission at multiple single-modes in a single DFB QCL has been demonstrated.<sup>11</sup> The device makes use of a grating with an aperiodic basis (GAB), which provides distributed feedback at several well-defined wavelengths. In these devices, as well as, in regular DFB QCLs, the output power and the selection of the actual lasing mode is sensitive to the phase shift of the radiation reflected from the uncoated end facets.<sup>6</sup> This reduces fabrication yield and reproducibility. While anti-reflection coatings have been employed for QCLs to mitigate these problems,<sup>6</sup> their use for broadband QCLs is limited by the availability of

IR-transparent materials and long-term reliability issues. In multi-wavelength DFBs,<sup>11</sup> the effect of the facet feedback is amplified by gain competition between the different grating modes. In this work, we use an external mirror positioned close to the back facet of the laser to modulate the feedback experienced by each mode and provide a post-fabrication control over the lasing modes. The effect of the small feedback modulation is amplified by gain competition, leading to a switching behavior between the individual grating modes of a multimode DFB QCL. By controlling the position of the external mirror, different modes or subsets of modes can be selected, with excellent extinction ratio. Our external micro-cavity QCL is free of any collimation optics and thus, compact and easy to align.

The QCL active region used for this work is a broadband bound-to-continuum design<sup>12</sup> operating around 8.4  $\mu\text{m}$ . It was grown by organometallic chemical vapor deposition on a conducting InP substrate.<sup>13</sup> Details on the grown layers and fabrication steps can be found in Ref. 11. The fabricated laser ridges (20, 23, and 26- $\mu\text{m}$ -wide) were cleaved to a length of 2.5 mm and indium mounted epi-side up on copper heat sinks. The QCLs are operated in pulsed mode at a repetition frequency of 20 kHz with a pulse duration of 50 ns.

Two types of gratings were fabricated. As a reference, we used a standard first-order single-mode DFB grating designed for operation at 1185  $\text{cm}^{-1}$ . For multi-mode operation, we used a DFB grating with an aperiodic basis,<sup>11</sup> providing distributed feedback for five equidistant modes separated by  $\approx 20 \text{ cm}^{-1}$  within the gain region of the material. Details on the grating sequence can be found in Ref. 11.

A microscale external cavity is formed by a gold mirror mounted on a piezo-stepper and initially positioned almost in contact with the uncoated laser back facet. A schematic of the setup is shown in inset of Fig. 1(a). During the experiment,

<sup>a)</sup>Electronic mail: capasso@seas.harvard.edu

the emission spectra of the QCLs were measured using a Fourier transform infrared spectrometer, while scanning the mirror position in sub-micrometer steps from a facet distance of less than  $1\ \mu\text{m}$  to about  $0.9\ \text{mm}$ . For each mirror position, the driving current was swept from threshold to rollover (maximum output power), resulting in a full parameter map of the devices performance. The output power was measured by a calibrated powermeter during a second current sweep.

Figures 1(a) and 1(b) show the dependence of the peak power of a single-mode DFB with the mirror position. For short cavities, the modulation of the output power can be understood by treating the external cavity like a lossy Gires–Tournois (GT) etalon,<sup>14,15</sup> where the high cavity losses stem from the large divergence of the uncollimated QCL output. When the DFB wavelength is on resonance with the lossy GT cavity, the power is efficiently coupled into the cavity. This results in a low effective reflectivity of the back facet-gold mirror system since the power is lost inside the external cavity (mainly because of the divergence of the beam and resulting low waveguide re-insertion), leading to a high threshold and a low peak power. Such resonant condition is reached whenever the external cavity length is an integer multiple of half the DFB wavelength, hence the  $4.2\ \mu\text{m}$

periodicity of the modulation. In Fig. 1(b), showing a zoom-in on the first few modulation periods, we observe sharp dips in peak power (and sharp peaks in threshold current) corresponding to these lossy resonances. From the width of the first dip, we estimate a quality factor of 6.

As the external cavity length is increased beyond the Rayleigh length of the uncollimated output beam, the finesse of the GT etalon drops rapidly, since less power is reinjected into the laser waveguide (see Fig. 1(a)). For a mirror distance of  $100\ \mu\text{m}$ , about 1% of the power emitted by the back facet actually hits the device facet after one round trip.<sup>17</sup> The peak power dips become accordingly broader. Eventually, when multiple reflections in the external cavity can be neglected, the peak power and current threshold modulations have a sine wave shape resulting from the interference between the back facet reflection and the small reinjected reflection from the external mirror. In this weak-coupling regime, the output power modulation is less than 10%.

Figure 2 shows the experimental results obtained for the multi-wavelength DFB. The black curve in Fig. 2(a) shows the spectrum of the original laser (without external feedback). While five Fourier peaks were designed to fall within the gain bandwidth, with their amplitude adjusted in an effort to reach a flat net gain for all five modes,<sup>11</sup> only four wavelengths are lasing simultaneously on this particular device, with one mode at  $\approx 1205\ \text{cm}^{-1}$  being significantly less powerful than the others. The number and subset of modes lasing simultaneously varies with drive current and from device to device, with a strong influence of the facet cleave position, as discussed later in the text.

With the introduction of the external mirror, each mode of this multi-wavelength DFB experiences an effective feedback from the composite system formed by the back cleaved facet and the external cavity. This feedback is modulated periodically as the external cavity length varies, with a period of  $\lambda_i/2$ , where  $\lambda_i$  is the wavelength of each mode. Corresponding oscillations in power output can be observed in Figs. 2(b) and 2(c). Interestingly, we note that even though the feedback provided by the external mirror is very small ( $R < 1\%$  for a cavity length of  $100\ \mu\text{m}$  and more), the observed intensity modulations are very deep, periodically switching off most modes. This is due to the fact that a small feedback difference can modify the competition between the DFB modes, resulting in one or two modes suppressing all the others. Such amplification of the modulation depth by mode competition is also responsible for the persistence of the modulation for larger cavity length close to  $1\ \text{mm}$ , where the feedback from the external mirror is very weak ( $R < 0.1\%$ ). As seen in Fig. 2(a), this results in true single-mode operation of the device at certain mirror positions. The wavelength of single-mode operation can be switched between the individual modes of the multi-mode DFB grating by varying the external cavity length.

To evaluate the mode selection capability, we find the most powerful mode at every mirror position and calculate its side-mode suppression ratio (SMSR). Results are shown in Fig. 2(d). While multi-mode operation (SMSR  $< 10\ \text{dB}$ ) is observed at a large number of mirror positions, the system features single-mode operation at certain cavity lengths for three of the DFB modes, with a SMSR larger than  $30\ \text{dB}$ . For

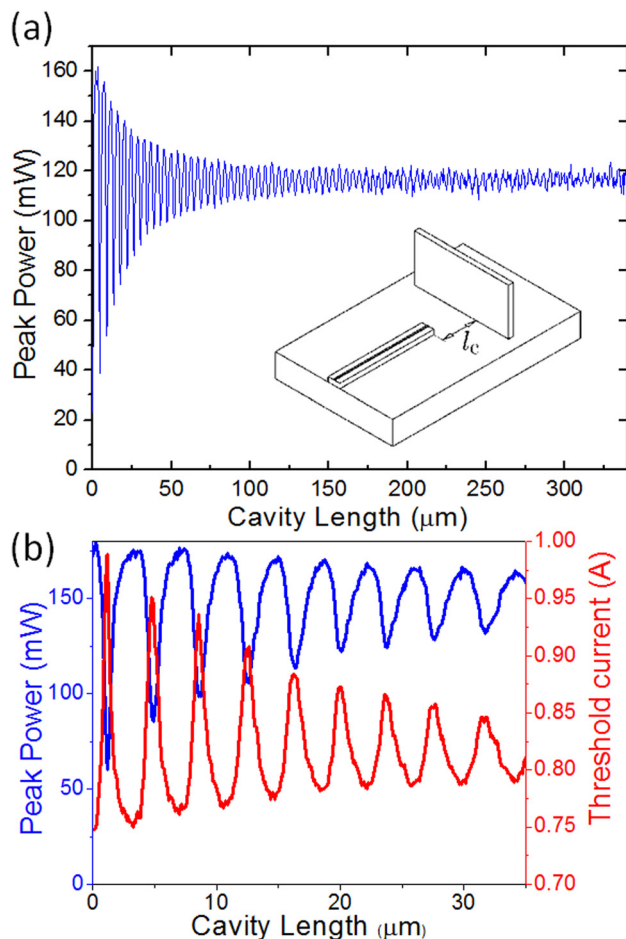


FIG. 1. (a) Measured modulation of the peak power of a single-mode DFB QCL with the external cavity length. Inset: Schematic of the experimental setup, with a laser bar mounted on a copper submount and a gold coated mirror in front of the uncoated back facet. The cavity length  $l_c$  is controlled by a piezo stepper. (b) Peak power and threshold current for short cavity lengths ( $0 < l_c < 30\ \mu\text{m}$ ).

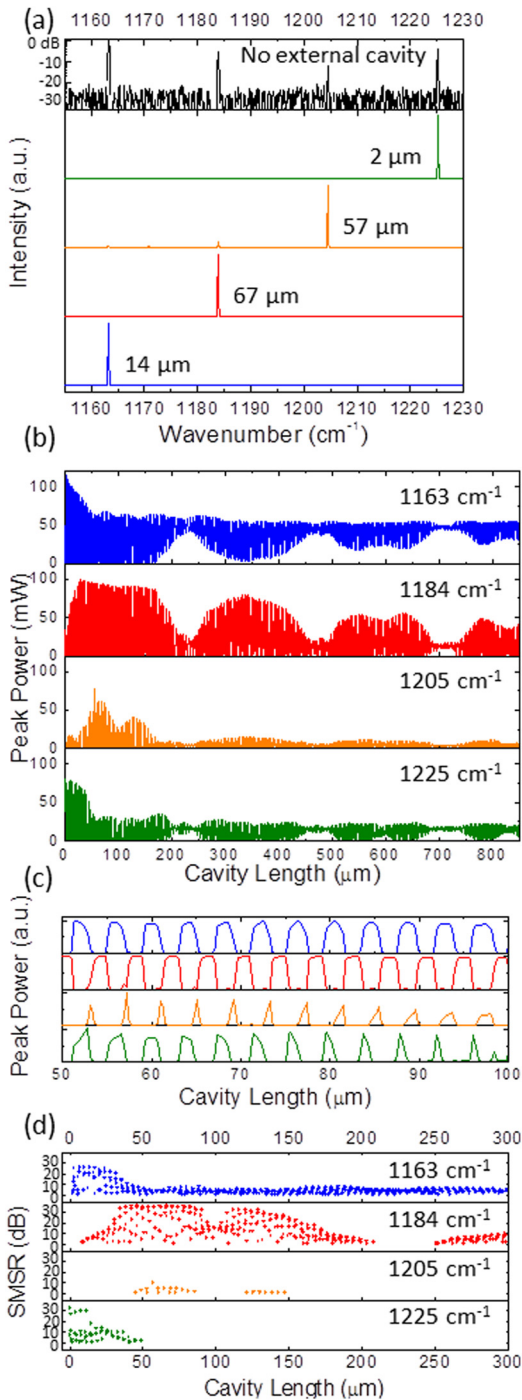


FIG. 2. (a) Spectra of the multi-wavelength DFB QCL. From top to bottom: Original laser (no external cavity) (black-log scale), laser with external cavity length  $l_c = 2 \mu\text{m}$  (green),  $l_c = 57 \mu\text{m}$  (orange),  $l_c = 67 \mu\text{m}$  (red), and  $l_c = 14 \mu\text{m}$  (blue). (b) Intensity modulation for the four lasing DFB modes with varying cavity length. The peak power values are obtained from the measured spectral intensity of the four modes. (c) Zoom-in of the modulation shown in Fig. 2(b), for external cavity length between  $50 \mu\text{m}$  and  $100 \mu\text{m}$ . The traces are normalized to emphasize the modulation depth of each mode. (d) Measured side-mode suppression ratio for the dominant mode at each mirror position.

the mode around  $1205 \text{ cm}^{-1}$ , true single-mode operation could not be achieved due to a persistent lasing of the modes at  $1184 \text{ cm}^{-1}$  and  $1163 \text{ cm}^{-1}$ . As seen from the spectrum recorded without an external cavity at the same driving current (Fig. 1(a)), the mode at  $1205 \text{ cm}^{-1}$  is the weakest mode without feedback.

We also note that there is a beat pattern in the modulation amplitude. Individual modes  $\lambda_i$  experience comparable feedback at mirror positions fulfilling  $l_c \approx m_i \lambda_i / 2$ , where  $m_i$  are integers. Certain mirror positions fulfill this condition for all wavelengths simultaneously, and slightly moving the mirror away from this position affects all of the modes equally. As a consequence, the influence of the external mirror on mode competition drops around these points, and the modulation amplitude decreases accordingly.

In order to gain insight into the behavior of the multi-wavelength laser, with and without external cavity, we used a linear model with gain first described by Ebeling and Coldren<sup>16</sup> and further detailed in supplementary material.<sup>17</sup> The system is described by a transfer matrix, and by solving an equation translating a self-oscillating condition, we obtain the longitudinal modes of the laser and their respective threshold gain (i.e., the material gain for which they start lasing). We can thus theoretically study the evolution of the lasing threshold for the five DFB modes of interest, as the cleaved facet positions or the external cavity length are varied.

Theoretical results on the influence of the cleave position (without external feedback) are shown in Fig. 3. The curves are normalized so that the five modes have the same threshold when the waveguide is cleaved exactly at the interface between two unit cells (i.e., no additional layer, as defined in Fig. 3(a)). This assumes perfect design of the grating so that all five modes experience the same net gain. According to the simulations, the threshold gain varies drastically with the cleave position (close to 10% in modulation amplitude), with very different profiles for the five modes of interest. The pattern repeats approximately periodically for added layer thickness spaced by  $\approx \lambda / 2n$ , where  $n$  is the refractive index of the added layer (QCL waveguide material,  $n = 3.18$  assumed here). Only the first period is shown in Fig. 3. The differences in the threshold dependence between the modes, as well as, the observed symmetries are related to

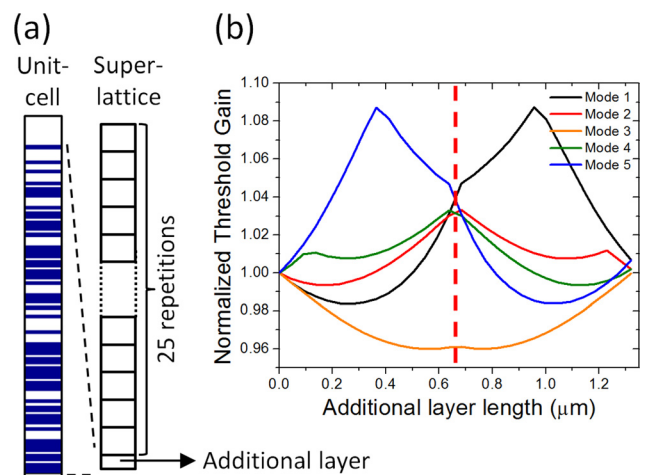


FIG. 3. (a) Schematic of the simulated DFB structure, with 25 repetitions of the unit cell, itself composed of 108 quarter layers with refractive index 3.16 or 3.18, arranged according to a Rudin-Shapiro sequence. An additional layer with refractive index 3.18 is included at the end of the designed grating to account for the cleave position uncertainty. (b) Calculated threshold gain, normalized so that all modes have identical threshold when no additional layer is present. The red vertical line indicates the layer thickness (660 nm) for which single wavelength lasing is the most likely, used for the results shown in Fig. 4(d).

the grating unit cell design. The equality in threshold between the five modes, as assumed for a perfect cleave position at the unit cell interface, degrades rapidly within 200 nm of additional layer thickness. Note that this is only a rough estimate, since it is not precisely known what threshold gain difference can be overcome by spatial hole burning and other instabilities or nonlinearities in the laser waveguide, in order to achieve multi-mode operation. The fact that the laser chosen here operates simultaneously on four modes without external feedback indicates that for this particular laser, the waveguide was cleaved close to an optimal position.

We then included the external mirror in the linear model. Results of the simulations are shown in Fig. 4. The experimental observations are well reproduced: For each mode with wavelength  $\lambda_i$ , the threshold is modulated with a period of  $\lambda_i/2$ . Two regimes can be distinguished: At short external cavity length (see Fig. 4(b)), the threshold gain features sharp peaks, revealing the feedback drop whenever a mode wavelength is on resonance with the lossy external cavity. As the quality factor of the lossy GT etalon decreases, the modulation approaches the shape of a sine wave (see Fig. 4(c)), characteristic of a simple interference between the

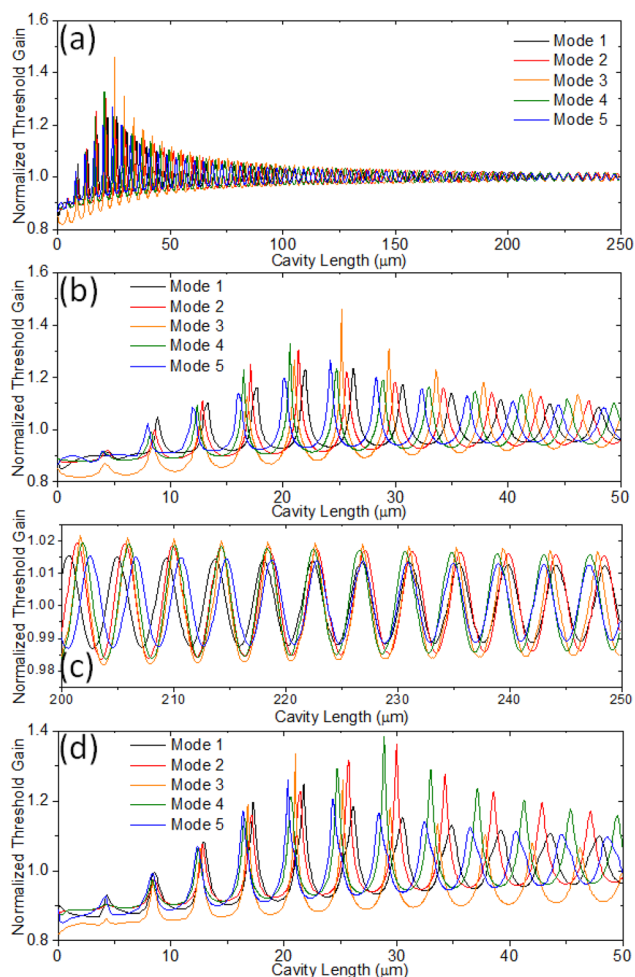


FIG. 4. Calculated threshold gain for different external cavity length  $l_c$ , normalized so that all five modes have identical threshold when no additional layer and no external cavity are present. (a)–(c) No additional layer is included (perfect cleave position). (d) With a 660 nm-thick additional layer added at the end of the laser waveguide, corresponding to the red line in Fig. 3(b).

light reflected by the laser back facet and the light reflected by the external mirror and reinjected into the waveguide. Assuming waveguide losses of  $10 \text{ cm}^{-1}$ , we obtain a threshold gain modulation by up to 50% in the strong feedback regime and of  $\approx 3.5\%$  around  $l_c = 250 \mu\text{m}$ . The experimentally observed beat pattern is also reproduced: The feedback modulation is in phase for the different modes for  $l_c = 225 \mu\text{m}$  (see Fig. 4(c)), in agreement with the experiment.

For the results shown in Figs. 4(a)–4(c), the positions of the facets are assumed to be perfect, i.e., exactly at the end of the designed grating. This is a realistic choice for the measured device since it originally lases on four modes, indicating a close to optimal cleave position. However, as discussed earlier, the cleave position will statistically be less optimal in most samples. In order to investigate the susceptibility of the observed effects to this parameter, we calculated the variations in threshold gain for the five DFB modes of interest in the case of a 660 nm-thick additional layer, which corresponds to the least favorable situation for multi-wavelength lasing (without external cavity), as indicated by Fig. 3(b) (vertical dashed red line). In such conditions, the original laser is expected to lase on a single-mode (referenced as mode 3 in Figs. 3 and 4). With the external cavity, this mode still has the lowest threshold for most mirror positions. However, for certain mirror positions within the plotted range ( $l_c \in [0, 50 \mu\text{m}]$ ), modes 1 and 5 show the lowest threshold, increasing the potential for single-mode operation on these modes. These positions are in the vicinity of the GT resonances for mode 3, where this mode experiences less feedback from the composite back facet.

In conclusion, we have demonstrated switching between individual wavelengths of a multi-wavelength DFB QCL by means of feedback from a short external lensless microcavity. We rely on gain competition between the individual DFB modes in order to achieve a 100% intensity modulation for each mode. The concept is robust against fabrication uncertainties such as the precise position of the cleaved facet and can offer a post-fabrication laser mode control. The switchable multi-wavelength QCL demonstrated here is suitable as a source for selected spectroscopic applications which require wavelength tuning in the vicinity of several well-defined frequencies in order to identify a chemical compound.

We acknowledge support from the Defense Threat Reduction Agency-Joint Science and Technology Office for Chemical and Biological Defense (Grant No. HDTRA1-10-1-0031-DOD). This work was performed in part at the Center for Nanoscale Systems (CNS) at Harvard University, a member of NNIN, which is supported by the NSF. P. Rauter acknowledges support from the Austrian Science Fund (FWF): No. J 3092-N19.

<sup>1</sup>R. F. Curl, F. Capasso, C. Gmachl, A. A. Kosterev, B. McManus, R. Lewicki, M. Pusharsky, G. Wysocki, and F. K. Tittel, *Chem. Phys. Lett.* **487**, 1 (2010).

<sup>2</sup>R. Martini, C. Bethea, F. Capasso, C. Gmachl, R. Paiella, E. A. Whittaker, H. Y. Hwang, D. L. Sivco, J. N. Baillargeon, and A. Y. Cho, *Electron. Lett.* **38**, 181 (2002).

<sup>3</sup>K. Fujita, T. Edamura, S. Furuta, and M. Yamanishi, *Appl. Phys. Lett.* **96**, 241107 (2010).

<sup>4</sup>Y. Yao, X. Wang, J.-Y. Fan, and C. Gmachl, *Appl. Phys. Lett.* **97**, 081115 (2010).

- <sup>5</sup>A. Hugi, R. Maulini, and J. Faist, *Semicond. Sci. Technol.* **25**, 083001 (2010).
- <sup>6</sup>B. G. Lee, M. A. Belkin, C. Pflügl, L. Diehl, H. A. Zhang, R. M. Audet, J. MacArthur, D. P. Bour, S. W. Corzine, G. E. Höfler, and F. Capasso, *IEEE J. Quantum Electron.* **45**, 554 (2009).
- <sup>7</sup>P. Rauter, S. Menzel, A. Goyal, B. Gokden, C. A. Wang, A. Sanchez, G. Turner, and F. Capasso, *Appl. Phys. Lett.* **101**, 261117 (2012).
- <sup>8</sup>T. Mansuripur, S. Menzel, R. Blanchard, L. Diehl, C. Pflügl, Y. Huang, J. H. Ryou, R. D. Dupuis, M. Loncar, and F. Capasso, *Opt. Express* **20**, 23339 (2012).
- <sup>9</sup>S. Slivken, N. Bandyopadhyay, S. Tsao, S. Nida, Y. Bai, Q. Y. Lu, and M. Razeghi, *Appl. Phys. Lett.* **100**, 261112 (2012).
- <sup>10</sup>P. Fuchs, J. Seufert, J. Koeth, J. Semmel, S. Hofling, L. Worschech, and A. Forchel, *Appl. Phys. Lett.* **97**, 181111 (2010).
- <sup>11</sup>R. Blanchard, S. Menzel, C. Pflügl, L. Diehl, C. Wang, Y. Huang, J.-H. Ryou, R. D. Dupuis, L. D. Negro, and F. Capasso, *New J. Phys.* **13**, 113023 (2011).
- <sup>12</sup>A. Wittmann, T. Gresch, E. Gini, L. Hvozdar, N. Hoyler, M. Giovannini, and J. Faist, *IEEE J. Quantum Electron.* **44**, 36 (2008).
- <sup>13</sup>Y. Huang, J.-H. Ryou, R. D. Dupuis, C. Pflügl, F. Capasso, K. Sun, A. Fischer, and F. Ponce, *J. Cryst. Growth* **316**, 75 (2011).
- <sup>14</sup>F. Gires and P. Tournois, "Interferometre utilisable pour la compression d'impulsions lumineuses modulees en frequence," *C. R. Acad. Sci. Paris* **258**, 6112–6615 (1964).
- <sup>15</sup>A. Yariv and P. Yeh, *Photonics: Optical Electronics in Modern Communications* (Oxford University Press, 2006), p. 167.
- <sup>16</sup>K. J. Ebeling and L. A. Coldren, *J. Appl. Phys.* **54**, 2962 (1983).
- <sup>17</sup>See supplementary material at <http://dx.doi.org/10.1063/1.4863663> for a detailed description of the simulation method.